Medicinal Chemistry Research (2026) 35:784–791
https://doi.org/10.1007/s00044-026-03556-z

MEDICINAL CHEMISTRY RESEARCH

BRIEF REPORT

Exploring $NiCl_2$, $PdCl_2$ and $PtCl_2$ as a catalyst for [3 + 2] cycloaddition in Kopsane alkaloid synthesis by density functional theory study

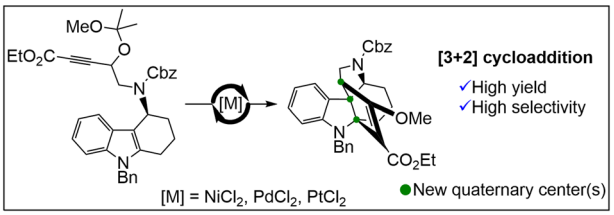
Sanghee Yoon[1] · Pratanphorn Nakliang[1] · Bilal Shaker[1] · Tao Ye[1,2] · Sun Choi[1]

Received: 12 February 2026 / Revised: 31 March 2026 / Accepted: 3 April 2026 / Published online: 21 April 2026
© The Author(s) 2026

Abstract

Kopsane alkaloids possess a complex heptacyclic scaffold and exhibit significant biological activities, including cholinergic, anti-inflammatory, and anti-cancer effects. While we previously reported $PtCl_2$-catalyzed [3 + 2] cycloaddition for their synthesis, the high cost and toxicity of platinum necessitate sustainable alternatives. In this study, we employed density functional theory (DFT) to investigate MCl_2 (M = Ni, Pd, and Pt) catalyzed [3 + 2] cycloaddition in Kopsane alkaloid synthesis. Our results indicate consistent reaction characteristics across all metals, with the second cyclization acting as the diastereoselectivity-determining step. The calculated energy gaps between transition states (TS2s) for $NiCl_2$, $PdCl_2$, and $PtCl_2$ were 5.57, 1.45, and 12.25 kcal/mol, respectively. These energy profiles suggest that $NiCl_2$ can achieve high diastereoselectivity similar to $PtCl_2$ due to its significant energy gap (> 4 kcal/mol). The implementation of this computational chemistry technique provides theoretical evidence that could help to improve the efficiency of the catalyst designing process.

Graphical Abstract



Keywords Kopsane alkaloids · Organic synthesis · Density functional theory · Catalyst design

Introduction

In the pharmaceutical industry, more than half of the available drugs are chiral compounds. Although two enantiomers have the same chemical structure, most of them display differences in biological activities such as pharmacology, toxicology, pharmacokinetics, metabolism, etc. Therefore, the enantiomerically pure synthesis is necessary to eliminate the production of unwanted isomer during preparation [1–3]. The selectivity of reactions has become a major interest for both academics and industry. A detailed understanding of chemical reactions is an essential piece of information that would help in the design of synthetic pathways, design of molecules that interact in specific ways with other molecules, develop a new catalyst, which provides a better specificity, etc [4–11]. In recent decades, computational simulation has been proved to be of high accuracy and precision. For example, the reactivity of a molecule can be obtained with reliable accuracy. It has been

✉ Sun Choi
sunchoi@ewha.ac.kr

[1] Global AI Drug Discovery Center, College of Pharmacy and Graduate School of Pharmaceutical Sciences, Ewha Womans University, Seoul, Republic of Korea

[2] State Key Laboratory of Chemical Oncogenomics, Peking University Shenzhen Graduate School, Xili, Nanshan District, Shenzhen, China

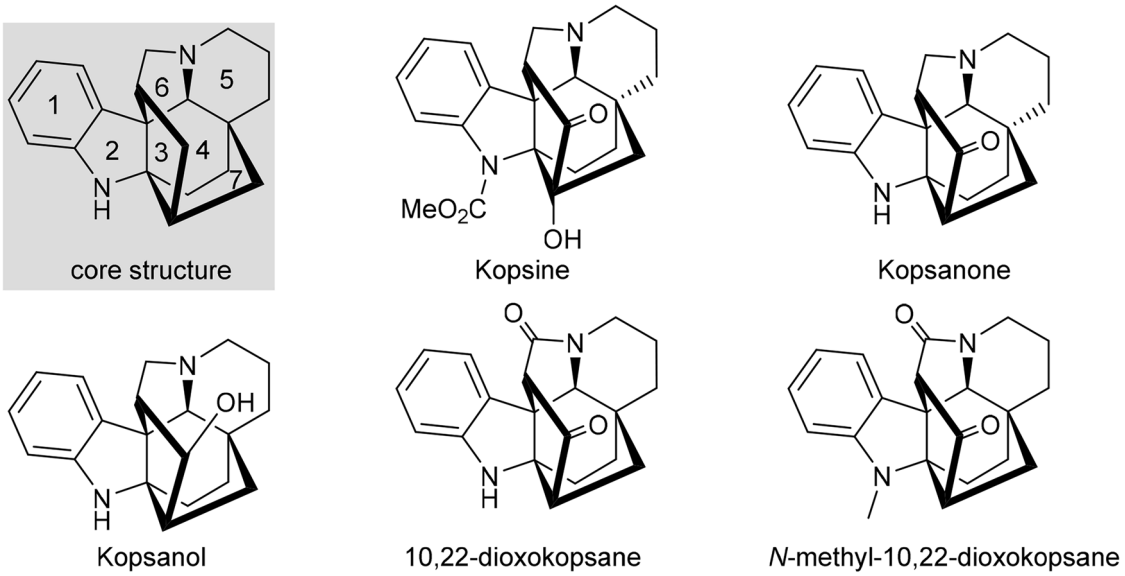


Fig. 1 Structure of the representative of Kopsane alkaloid compounds

used to verify the catalytic reactions that provide insights into the mechanistic features, including the catalytic process and selectivity of products. A short-life species (e.g. transition state) can be captured theoretically, which provides useful information in mechanistic study. However, it is very important to choose the most suitable computational method to investigate a specific chemical problem [12, 13]. The computational simulation of the possible reaction pathways enables to achieve an atomistic understanding of the reaction features. To date, computational simulation has also been used as a prediction tool rather than only rationalization, which serve as a rational starting point for experimental work.

The kopsane alkaloids are a family of natural products that are derived from Kopsia plant available in China, Southeast Asia, South Asia, and some parts of Australia [14–17]. Several studies showed that they have interesting biological activities including antitumor, antimanic, antitussive, and antileishmanial effects, and have been used for the treatment of dropsy and rheumatoid arthritis[18, 19]. The core structure of these compounds consists of a rigid heptacyclic framework composed of seven fused rings and several stereogenic centers,typically six to seven depending on the derivative. This highly congested polycyclic architecture renders the synthesis of kopsane alkaloids particularly challenging and has attracted significant interest in synthetic methodology development (Fig. 1). Therefore, the major challenge for synthetic chemists is the construction of this polycyclic skeleton. One of the common techniques is the transition-metal catalyzed cycloaddition reactions. To date, noble metal catalysts dominated the cycloaddition [20–22]. For instance, Zhang's group reported the Pt(II) catalyzed indole-fused structure using intramolecular [3 + 2] cycloaddition compared to their previous Au(I)-catalyzed similar reactions. Different products were obtained depending on the metal and condition used [23–25]. Pt(II)-catalyst was applied to catalyze the [3 + 2] cycloaddition of α,β-unsaturated carbene intermediates from diverse propargyl ethers. It is an important step in the formation of polycyclic compounds in high yield and selectivity [26]. In 2015, Mei and co-workers showed that the stereo- and regioselectivity of indole-fused synthesis are catalyst-dependent. The [3 + 2] cycloaddition proceeded when an Au- or Pt-catalyst was used, while [2 + 2] cycloaddition took place in the presence of IPrAuCl and $AgNTf_2$ [27].

In this communication, we would like to point out a practical use of computational simulation that explores reaction mechanisms and helps rationalize experimental observations, and drives laboratory experiments by predicting synthetic ability [8, 9, 11, 28, 29]. In 2020, Jia and coworkers reported that the combination of $PtCl_2$ and 4 Å molecular sieve in dichloroethane at 85 °C and reflux condition delivered great stereoselectivity of [3 + 2] cycloaddition reaction of indole alkyne substrates, which is a molecular scaffold of Kopsane alkaloids [30]. The key step of synthesis is depicted in Fig. 2, where the vicinal quaternary centers and two rings are formed in a single step. A plausible catalytic mechanism begins with the initial coordination of Pt-catalyst to the triple bond (I), followed by the intramolecular nucleophilic attack of methoxy group that results in III and acetone. Then, it subsequently undergoes [3 + 2] cycloaddition that V is obtained. However, Pt metal is extremely expensive and environmentally toxic.

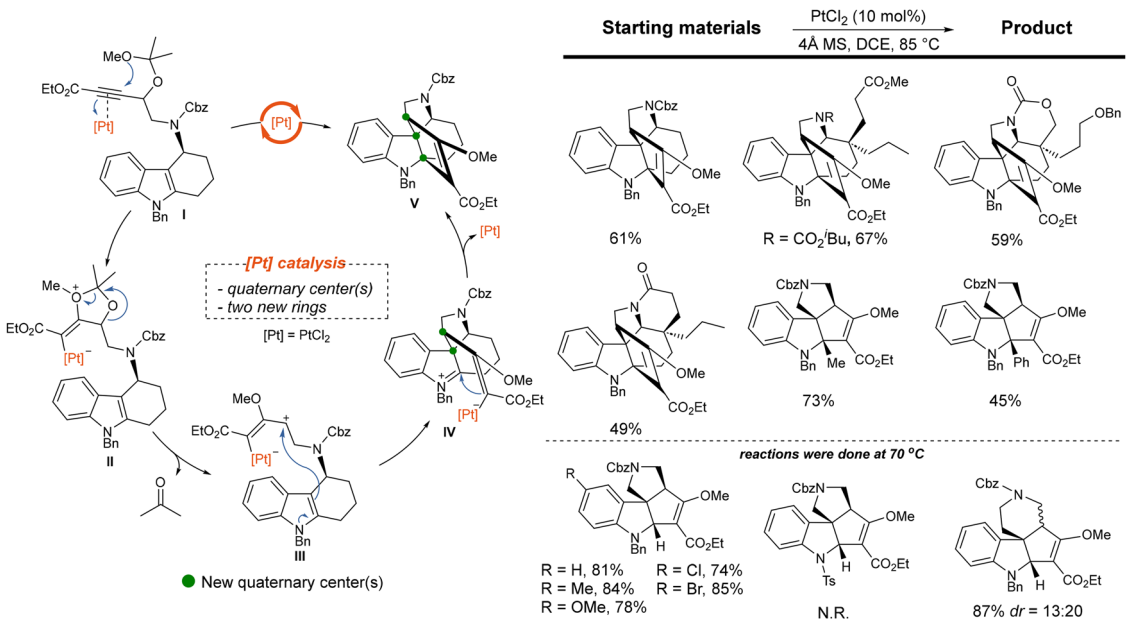


Fig. 2 $PtCl_2$ catalyzed [3 + 2] cycloaddition in Kopsane alkaloids synthesis (ref. 30)

Therefore, using the same group metals (Pd and Ni), which are cheaper could be an alternative solution for this issue. Thus, we exploited computational simulations to verify the reaction profiles and rationalize the possibility of replacing Pt with other group 10 metals.

Results and discussion

$PtCl_2$ catalyst

The energy diagram for $PtCl_2$-catalyzed reaction is shown in Fig. 3a. The reactant complexes (RC) employed in this study represent the metal-activated 1,3-dipole intermediates generated upon coordination of $PtCl_2$ to the alkyne moiety, which correspond to the key intermediate proposed in the previously reported catalytic mechanism [30]. Throughout this study, the notation P(*R*,*R*) and P(*R*,*S*) refers to the configurations at C3 and C7, respectively. The first descriptor denotes the stereochemistry established during the first cyclization step (C3-C7 bond formation) and the second descriptor denotes that established during the second cyclization step (C2-C9 bond formation). These correspond to P(*3 R*,*7 R*) and P(*3 R*,*7S*).

The RCs for the two pathways are comparable, with a difference in relative energy of less than 1 kcal/mol at the level of theory used. The first cyclization is almost barrierless ($\Delta G^{\ddagger} < 2$ kcal/mol). This step yields relatively stable intermediate 1 (Int1), which also provides two different C7 diastereomeric intermediates. It was found that the $\Delta G^{\ddagger}$ of TS1s are approximately equal, which revealed that the first step is competitive between C7(*R*-) and C7(*S*-) formation. The second ring formation is the rate-determining step and distinguished between two diastereomeric products. The $\Delta\Delta G^{\ddagger}$ between the two diastereomeric TS2s was 12.25 kcal/mol, favoring the P(*R*,*R*) pathway and consistent with the observed sole product of P(*R*,*R*). The P(*R*,*R*) Int2 is more stable than that of P(*R*,*S*), indicating that the reverse reaction is more difficult for P(*R*,*R*) path. Moreover, the P(*R*,*R*) proceeded through TS3 and yielded stable Int3 that $PtCl_2$ coordinates to the indole moiety. Compared to the P(*R*,*S*) path, the TS3 of P(*R*,*R*) was 9.02 kcal/mol lower. Thus, P(*R*,*R*) is favorable due to kinetic (TS2 and TS3) and thermodynamics controls (Int2 and Int3).

Close examination of each reaction path revealed several explanations for stereoselectivity. The first [3 + 2] cyclization occurs at the cation C7 and electron-rich C3. This step is facile due to the low steric and pre-chiral *S*-C3 which is pointing to the beta-face of the indole plane. Without any hindrance, both *R*-C7 and *S*-C7 formations are comparable. As shown in Fig. 3a, the Int1s have relatively low energy (~ −10 kcal/mol). Both intermediates showed similar stability. The obtained chiral C7 from the first ring formation causes the different conformation of Int1. The Int1 undergoes another [3 + 2] cyclization where the C2-C9 bond is formed. The difference in energy between both TS2s shows that the P(*R*,*R*) product is preferred. We determined the structures of two-diastereomeric transition state, and cause of difference in energy. Several interesting points were drawn: 1) The initial conformation of C7 at Int1 caused the steric hindrance for the C2-C9 bond formation. The side chain of P(*R*,*R*)-Int1 is directed to the C2 position that is ready to form a new bond, whereas the positions of the side

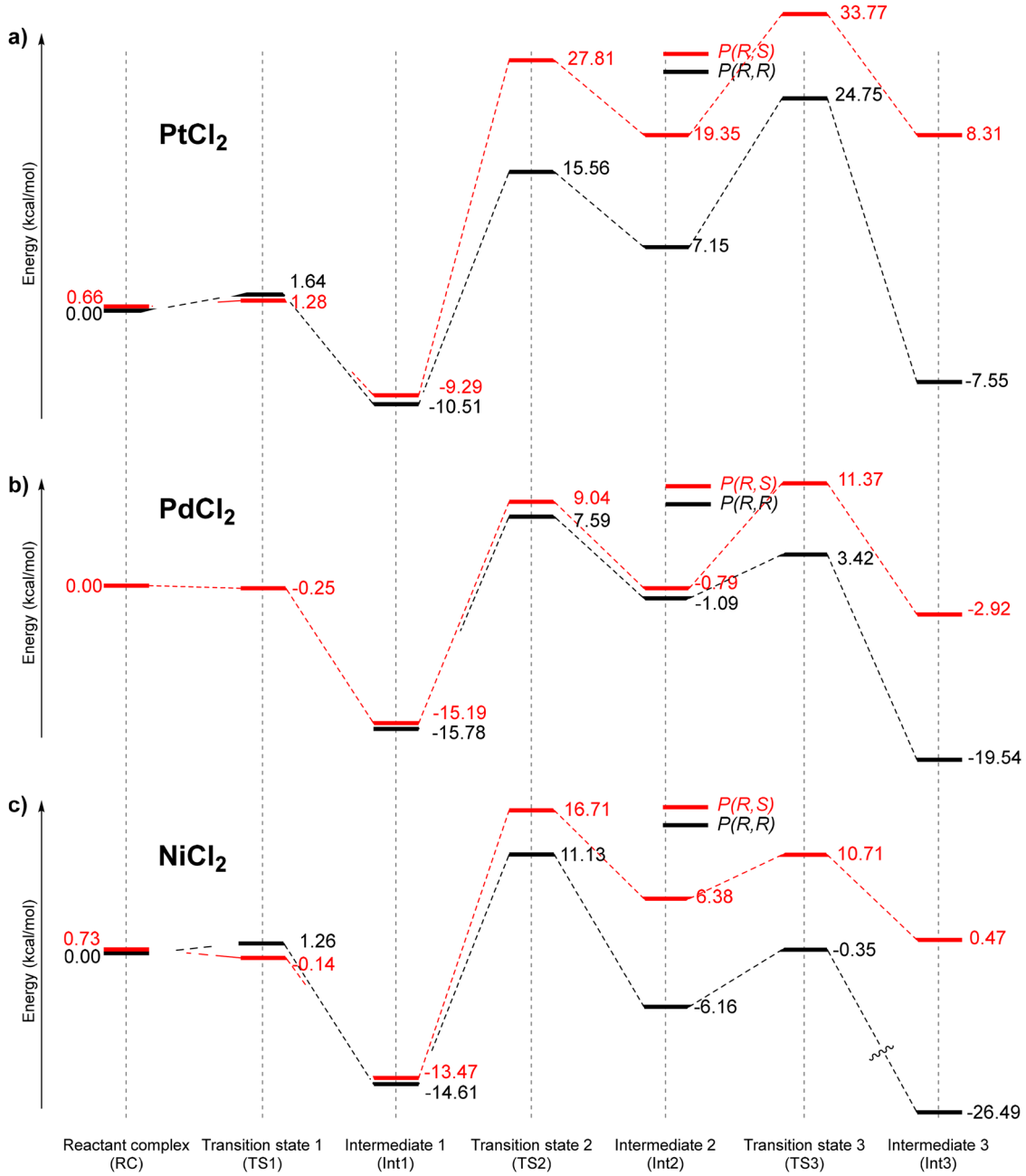


Fig. 3 Full energy diagrams of **a**) $PtCl_2$-catalyzed reaction, **b**) $PdCl_2$-catalyzed reaction, and **c**) $NiCl_2$-catalyzed reaction, as determined at the B3LYP(SCRF)/[SDD(metal atom), 6-311 + G(d,p)(others)]//B3LYP/[SDD(metal atom), 6-31 G(d,p) (others)]

chain and hydrogen atom of P(*R*,*S*)-Int1 are switched. Therefore, this cost more energy for the P(*R*,*S*) path to overcome the steric hindrance. 2) The frontier molecular orbital analysis found that the LUMO is located around the indole N atom for both cases, while the HOMO is different (Supporting information). In the case of P(*R*,*R*)-Int1, the HOMO is located along the π-orbital of the C8-C9 bond and non-bonding electrons of $PtCl_2$ moiety, which is ready to form a bond between C2 and C9. Meanwhile, HOMO of P(*R*,*S*)-Int1 is only located on the non-bonding orbital of $PtCl_2$ moiety that is not suitable for bond formation. However, the electron of π-orbital along the C8-C9 bond is found to be the HOMO-1, which has lower energy. As shown in Fig. 4, the charge distributions at C2 are almost identical for all paths, while the C9 is more negative for P(*R*,*R*) path indicating that more electrons were located on this carbon. Hence, the C9 is more reactive for nucleophilic attack reaction. Therefore, both charge and frontier molecular orbital analysis are complementary tools in determining chemical reactivity.

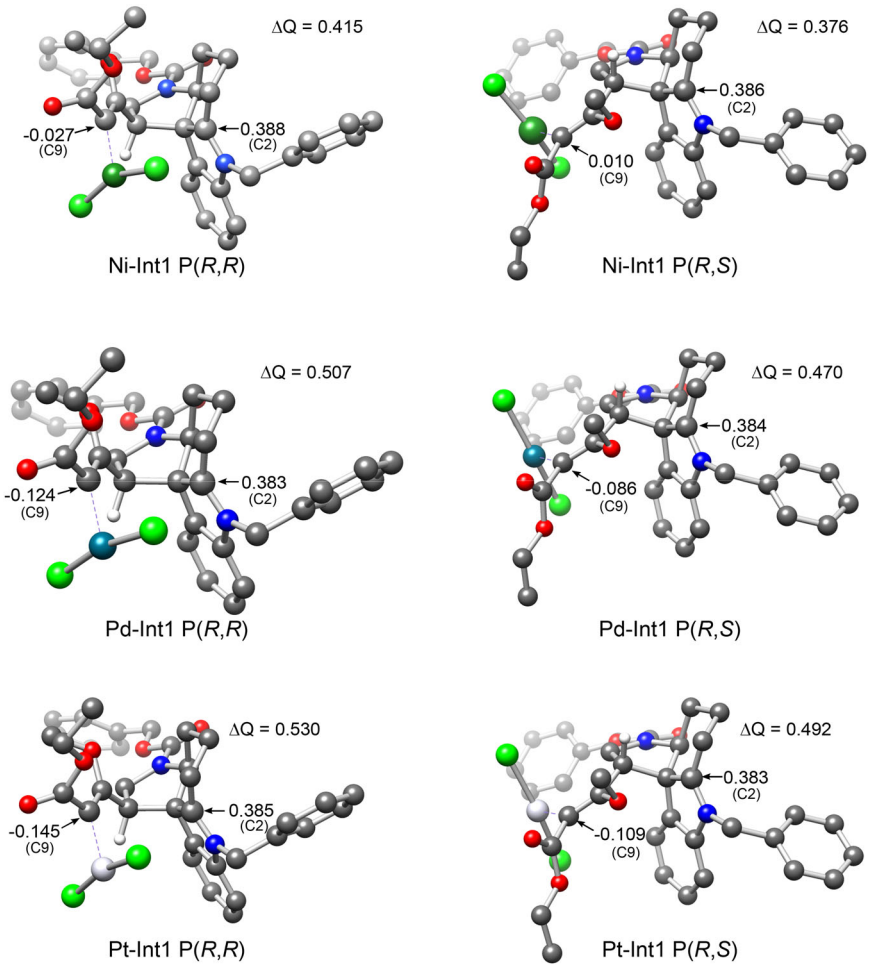


Fig. 4 Charge distribution (Q) and charge difference (ΔQ) of C2 and C9 of intermediate 1 calculated at B3LYP(SCRF)/[SDD(metal atom), 6-31 G(d,p) (others)] level

$PdCl_2$ catalyst

The energy diagram for $PdCl_2$ is presented in Fig. 3b. The Pt(II) center was replaced by Pd(II), which is in the same group. Surprisingly, only RC of P(R,S) was obtained. Nevertheless, the $\Delta G^{\ddagger}$ of TS1 is lower than that of RC (−0.25 kcal/mol) at the level of theory used. Therefore, the first ring formation is rather barrierless. The energy level of both Int1s is approximately equal (~−15 kcal/mol). Again, the second cyclization is the stereoselective step. The relative energies of TS2 are 7.59 and 9.04 kcal/mol for P(*R*,*R*) and P(*R*,*S*), respectively. The products have a slightly lower energy than that of RC. According to the energy diagram, the smaller energy gap between the two diastereomeric TS2s indicated a lower selectivity of the catalyst.

The structural observation provided similar aspects as found when $PtCl_2$ was a catalyst. Even though the RC was found in the case of the P(*R*,*S*) path, the free energy profile showed that there is no energy required for the first cyclization. The Int1s are much more stable compared to the RC. The second cyclization required around 23–25 kcal/mol of energy with respect to each Int1. The energy gap between two diastereomeric TSs is around 1.45 kcal/mol, which resulted in a theoretical diastereomeric ratio of 93.5:6.5 with P(*R*,*R*) preferred. However, the TS3 differentiated between two pathways. The TS3 of P(*R*,*R*) is more favorable by 7.95 kcal/mol. This leads to relatively stable Int3 in P(*R*,*R*).

A comparison of the energy diagrams for $PtCl_2$ and $PdCl_2$ catalyzed [3 + 2] cycloadditions showed that the C3-C7 bond formation is much easier for the $PdCl_2$ catalyst that is barrierless. Even though the energy gap of TS3s and Int3 are suggested that sole product could be obtained, the energy gap between TS2s in $PdCl_2$-catalyzed reaction is smaller, hence suggesting that $PdCl_2$ could provide less stereoselective products. In addition, the highest activation energy of $PdCl_2$ catalyzed reactions is lower than that of $PtCl_2$. It suggested that this reaction requires less energy to achieve the product.

$NiCl_2$ catalyst

Similar to the $PtCl_2$ catalyzed reaction, the RC of P(*R*,*R*) is the most stable, with RC of P(*R*,*S*) lying slightly higher in energy (Fig. 3c). The subsequent cyclization through TS1 has a very low energy barrier or nonexistent for P(*R*,*R*) and P(*R*,*S*), respectively. The first cyclization leads to the formation of the

C3-C7 bond. After Int1, the second step is still the rate-determining step for this reaction. The second cyclization required 25.74 and 30.18 kcal/mol of energy with respect to each Int1 for P(*R*,*R*) and P(*R*,*S*), respectively. These energy barriers are of similar magnitude to that of $PtCl_2$ catalyzed reaction. However, the relative energy level of TS2 is much lower at the theory level used. The energy gap between the two diastereomeric TSs is around 5.57 kcal/mol, which indicates the theoretical sole product of P(*R*,*R*) would be obtained. The P(*R*,*R*)-Int2 is relatively stable than RC. The relative barrier of P(*R*,*R*)-TS3 to Int2 is 5.81 kcal/mol. Compared to P(*R*,*S*), the P(*R*,*S*)-TS3 is around 11 kcal/mol higher. Finally, this result is consistent with the $PtCl_2$-catalyzed reaction.

A comparison of the energy diagrams clearly shows that the reaction features are similar for both $PtCl_2$ and $NiCl_2$-catalyzed reactions. Similar situations were found for the first step where the P(*R*,*S*)-TS1 has a lower energy barrier. Nevertheless, the P(*R*,*R*) Int1 is slightly more stable ($\Delta G < 1$ kcal/mol). The sole product could be obtained using $NiCl_2$ catalyst according to a large energy gap between the diastereoselective TSs (TS2). Moreover, the activation energies are lower than that of $PtCl_2$ catalyzed reactions. Thus, the $NiCl_2$ catalyst could therefore be used as a catalyst, replacing the expensive $PtCl_2$ catalyst.

Summary of the theoretical catalyst determination

Our comparative study shows that the MCl_2 catalyzed [3 + 2] cycloaddition reactions have the same reaction features that two rings are subsequently formed. The energy barriers for the first cyclization step are small or non-existent. Additionally, there is no RC found in the $PdCl_2$ catalyzed P(R,R) path. The rate-determining and diastereomeric-selective step is the second cyclization. The relative energy barriers of diastereomeric TS2 of P(*R*,*R*) and P(*R*,*S*) distinguish the product formation. The lower energy barrier pathway is preferred. Thus, it was found that the P(*R*,*R*) is the most favorable pathway for all the catalysts used. Therefore, either Ni or Pd can be used as a substituted catalyst in this [3 + 2] cycloaddition. A comparison of the calculated TS2 energy gap clearly shows that, among them, Ni(II) is a better replacement for this reaction due to a higher energy gap compared to Pd(II). Moreover, the reverse reaction from product shows that the reverse $NiCl_2$-catalyzed P(*R*,*R*) is much slower than P(*R*,*S*) due to higher reverse barrier energy.

Conclusion

In conclusion, we have performed DFT calculations to investigate the reaction mechanism of group 10 metal catalyzed [3 + 2] cycloaddition for $PtCl_2$ replacement. Several insights could be drawn from our study. The replacement of Pt(II) by Pd(II) or Ni(II) does not change the reaction features of [3 + 2] cycloaddition of Kopsane alkaloid synthesis. The low (or barrierless) first ring cyclization of all MCl_2-catalyzed reactions indicates that this step is fast and difficult to control. The rate-determining and diastereoselective step is the second-ring cyclization. All the P(*R*,*R*) pathways have lower barrier indicating that there is no difference in the preferable product for each catalyst. The close examination of Int1-charge distribution and their geometries draw a conclusion that both electronic and steric factors are involved in the diastereomeric selectivity of this reaction. The energy comparison between each reaction path suggested that $NiCl_2$ is a better replacement due to a higher ΔG-TS2 than that of $PdCl_2$. Moreover, the energy profiles of $NiCl_2$ catalyzed reactions are more similar to $PtCl_2$ than that of $PdCl_2$. These suggestions can be used as a rational starting point for further experimental works. These computational results provide mechanistic insight and suggest that $NiCl_2$ could be a promising and more sustainable alternative to $PtCl_2$. However, further experimental studies will be necessary to validate these theoretical predictions and evaluate the practical catalytic performance.

Methods

The [3 + 2] cycloaddition step of the kopsane alkaloid synthesis was investigated using the density functional theory (DFT). The MCl_2 (M = Ni, Pt, and Pd) was used as a catalyst (Fig. 5). There are two cyclization steps; i) C3-C7

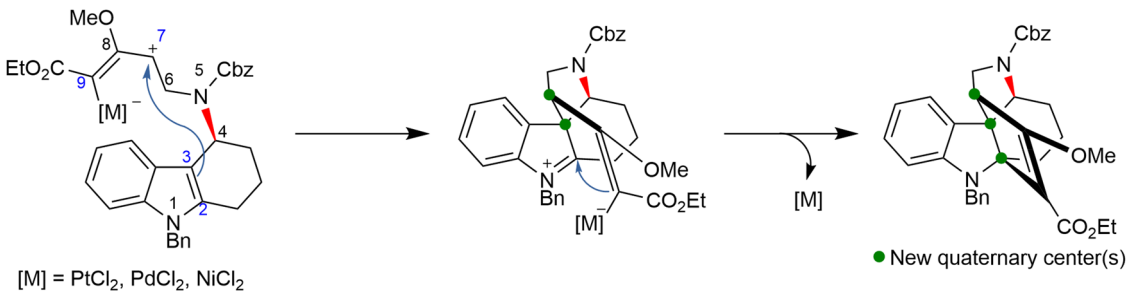


Fig. 5 [3 + 2] cycloaddition reaction mechanism

bond formation, and ii) C1-C9 bond formation that provided two new pentacyclic rings. All DFT calculations were performed using Gaussian 16 [31]. The B3LYP(SCRF)/[SDD(metal atom), 6-311 + G(d,p)(others)]//B3LYP/[SDD(metal atom), 6-31 G(d,p)(others)] method was used for geometry optimization and frequency calculations [12, 32–36]. The self-consistent reaction field (SCRF) implicit solvation model was used for the solvation effects in 1,2-dichloroethane ($\varepsilon = 10.125$) to imitate the experimental condition [37]. Frequency calculations were performed at the same level of theory to confirm the minima (no imaginary frequencies) or transition states (one imaginary frequency) and to obtain zero-point vibrational energy (ZPE) corrections. Thermal corrections were computed at 298.15 K and 1 atm pressure.

From the theoretical point of view, the selectivity is related to the difference in Gibbs free energies of the transition state in each product formation [35]. The probability of existence for the transition states of each product formation is written as:

$$P(A_i) = \sum_i exp^{-\Delta\Delta G^{\ddagger}_{A_i}/RT}$$

$$\%product = \frac{\sum_i P(A_i \, or \, B_i)}{\sum_i P(A_i) + \sum_i P(B_i)} \times 100$$

$$\%ee = \frac{\sum_i P(A_i) - \sum_i P(B_i)}{\sum_i P(A_i) + \sum_i P(B_i)} \times 100$$

where A and B are different diastereomers, $P(A_i)$ and $P(B_i)$ are Boltzmann distribution of existence for the i^{th} transition state of each product formation, and $\Delta\Delta G^{\ddagger}$ is the Gibbs free energy relative to the most stable transition state, R is the gas constant, and T is the temperature in K (298.15 K).

Data Availability

All data supporting the findings of this study are available within the paper and its Supplementary Information.

Supplementary information The online version contains supplementary material available at https://doi.org/10.1007/s00044-026-03556-z.

Acknowledgements This work was supported by the National Research Foundation of Korea (NRF) grant funded by the Korea government (MSIT) (RS-2026-25477010), Bio & Medical Technology Development Program (NRF-2022M3E5F3080873), and Brain Pool Program (RS-2023-00260706). We also thank the Korea Institute of Science and Technology Information (KISTI) Supercomputing Center for providing computing resources (KSC-2024-CRE-0552, KSC-2025-CRE-0418), and a Peng Cheng Scholar (to S.C.).

Author contributions The manuscript was written through contributions of all authors. All authors have given approval to the final version of the manuscript.

Funding Open Access funding enabled and organized by Ewha Womans University.

Compliance with ethical standards

Conflict of interest The authors declare no competing interests.

Publisher's note Springer Nature remains neutral with regard to jurisdictional claims in published maps and institutional affiliations.

Open Access This article is licensed under a Creative Commons Attribution-NonCommercial-NoDerivatives 4.0 International License, which permits any non-commercial use, sharing, distribution and reproduction in any medium or format, as long as you give appropriate credit to the original author(s) and the source, provide a link to the Creative Commons licence, and indicate if you modified the licensed material. You do not have permission under this licence to share adapted material derived from this article or parts of it. The images or other third party material in this article are included in the article's Creative Commons licence, unless indicated otherwise in a credit line to the material. If material is not included in the article's Creative Commons licence and your intended use is not permitted by statutory regulation or exceeds the permitted use, you will need to obtain permission directly from the copyright holder. To view a copy of this licence, visit http://creativecommons.org/licenses/by-nc-nd/4.0/.

References

1. Stevens JL. Future of toxicologymechanisms of toxicity and drug safety: where do we go from here?. Chem Res Toxicol. 2006;19:1393–401.
2. van Gunsteren WF, Bakowies D, Baron R, Chandrasekhar I, Christen M, Daura X, et al. Biomolecular modeling: goals, problems, perspectives. Angew Chem Int Ed. 2006;45:4064–92.
3. Mullard A. Biotech R&D spend jumps by more than 15%. Nat Rev Drug Discovery. 2016;15:447–447.
4. Durand DJ, Fey N. Computational ligand descriptors for catalyst design. Chem Rev. 2019;119:6561–94.
5. Wheeler SE, Seguin TJ, Guan Y, Doney AC. Noncovalent interactions in organocatalysis and the prospect of computational catalyst design. Acc Chem Res. 2016;49:1061–9.
6. Rohmann K, Hölscher M, Leitner W. Can contemporary density functional theory predict energy spans in molecular catalysis accurately enough to be applicable for in silico catalyst design? a computational/experimental case study for the ruthenium-catalyzed hydrogenation of olefins. J Am Chem Soc. 2016;138:433–43.
7. Grabow, LC, CHAPTER 1 Computational Catalyst Screening, in *Computational Catalysis*. 2014, The Royal Society of Chemistry. p. 1-58.
8. Houk KN, Cheong PHY. Computational prediction of small-molecule catalysts. Nature. 2008;455:309–13.
9. Nakliang P, Yoon S, Choi S. Emerging computational approaches for the study of regio- and stereoselectivity in organic synthesis. Org Chem Front. 2021;8:5165–81.
10. Hadadi N, Hatzimanikatis V. Design of computational retrobiosynthesis tools for the design of de novo synthetic pathways. Curr Opin Chem Biol. 2015;28:99–104.

11. Cheng G-J, Zhang X, Chung LW, Xu L, Wu YD. Computational organic chemistry: bridging theory and experiment in establishing the mechanisms of chemical reactions. J Am Chem Soc. 2015;137:1706–25.
12. Mardirossian N, Head-Gordon M. Thirty years of density functional theory in computational chemistry: an overview and extensive assessment of 200 density functionals. Mol Phys. 2017;115:2315–72.
13. *Organic and Bio-molecular Chemistry*. Vol. 2. 2009, Singapore: Eolss publisher. 434.
14. Mohammed AE, Abdul-Hameed ZH, Alotaibi MO, Bawakid NO, Sobahi TR, Abdel-Lateff A, et al. Chemical diversity and bioactivities of monoterpene indole alkaloids (MIAs) from six apocynaceae genera. Molecules. 2021;26:488.
15. Cheenpracha S, Raksat A, Ritthiwigrom T, Laphookhieo S. Monoterpene indole alkaloids from the twigs of kopsia arborea. Nat Product Commun. 2014;9:1934578X1400901010–3.
16. Kam T-S, Lim K-H Chapter 1 Alkaloids of Kopsia. In: Cordell GA, editor., The Alkaloids: Chemistry and Biology. Academic Press; 2008. pp. 1–111.
17. Yap W-S, Gan CY, Low YY, Choo YM, Etoh T, Hayashi M, et al. Grandilodines A−C, biologically active indole alkaloids from kopsia grandifolia. J Nat Products. 2011;74:1309–12.
18. Chen J, Yang ML, Zeng J, Gao K. New broad-spectrum antibacterial and antifungal alkaloids from Kopsia hainanensis. Phytochemistry Lett. 2014;7:156–60.
19. Chi WQ, Jiang YH, Hu J, Pan J. Cytotoxic and antibacterial aspidofractinine alkaloids from Kopsia hainanensis. Fitoterapia. 2018;130:259–64.
20. Qin B, Wang Y, Wang X, Jia Y. Total synthesis of kopsine, fruticosine, and structurally related polycyclic caged Kopsia indole alkaloids. Org Chem Front. 2021;8:369–83.
21. Anand A, Singh P, Kumar V, Bhargava G. Transition metal catalyzed [6 + 2] cycloadditions. RSC Adv. 2019;9:25554–68.
22. Kuila B, Kaur M, Singh P, Bhargava G. Transition-Metal-Catalyzed [3 + 2 + 2] Cycloaddition Reactions. Eur J Org Chem. 2018;2018:853–68.
23. Zhang LM. Tandem Au-catalyzed 3,3-rearrangement-[2 + 2] cycloadditions of propargylic esters: Expeditious access to highly functionalized 2,3-indoline-fused cyclobutanes. J Am Chem Soc. 2005;127:16804–5.
24. Zhang G, Catalano VJ, Zhang L. PtCl2-catalyzed rapid access to tetracyclic 2, 3-indoline-fused cyclopentenes: reactivity divergent from cationic Au (I) catalysis and synthetic potential. J Am Chem Soc. 2007;129:11358–9.
25. Zhang G, Zhang L. Au-containing all-carbon 1, 3-dipoles: generation and [3 + 2] cycloaddition reactions. J Am Chem Soc. 2008;130:12598–9.
26. Saito K, Sogou H, Suga T, Kusama H, Iwasawa N. Platinum(II)-Catalyzed Generation and [3 + 2] cycloaddition reaction of alpha,beta-unsaturated carbene complex intermediates for the preparation of polycyclic compounds. J Am Chem Soc. 2011;133:689–91.
27. Mei LY, Wei Y, Tang XY, Shi M. Catalyst-Dependent stereodivergent and regioselective synthesis of indole-fused heterocycles through formal cycloadditions of indolyl-allenes. J Am Chem Soc. 2015;137:8131–7.
28. Bachrach, SM, Computational organic chemistry. Annu Rep Sect "B" (Organic Chemistry), 2010. **106**: 407-27.
29. Mita T, Harabuchi Y, Maeda S. Discovery of a synthesis method for a difluoroglycine derivative based on a path generated by quantum chemical calculations. Chem Sci. 2020;11:7569–77.
30. Jia X, Lei H, Han F, Zhang T, Chen Y, Xu Z, et al. Asymmetric total syntheses of kopsane alkaloids via a PtCl2 -Catalyzed Intramolecular [3 + 2] Cycloaddition. A. ngew Chem Int Ed Engl. 2020;59:12832–6.
31. Frisch, MJ, et al., *Gaussian 16 Rev A03*. 2016: Wallingford, CT.
32. Dolg M, Wedig U, Stoll H, Preuss H. Energy-adjusted ab initio pseudopotentials for the first row transition elements. J Chem Phys. 1987;86:866–72.
33. Dunning TH, Hay PJ Gaussian Basis Sets for Molecular Calculations. In: Schaefer HF, editor., Methods of Electronic Structure Theory. Boston, MA: Springer US; 1977. pp. 1–27.
34. Ehlers AW, Böhme M, Dapprich S, Gobbi A, Höllwarth A, Jonas V, et al. A set of f-polarization functions for pseudo-potential basis sets of the transition metals Sc Cu, Y Ag and La Au. Chem Phys Lett. 1993;208:111–4.
35. Sameera WMC, Maseras F. Transition metal catalysis by density functional theory and density functional theory/molecular mechanics. Wiley Interdiscip Reviews-Computational Mol Sci. 2012;2:375–85.
36. Wadt WR, Hay PJ. Ab initio effective core potentials for molecular calculations. Potentials for main group elements Na to Bi. J Chem Phys. 1985;82:284–98.
37. Tomasi J, Mennucci B, Cammi R. Quantum mechanical continuum solvation models. Chem Rev. 2005;105:2999–3094.